COMMUNICATION

Check for updates

Application of a chemical clock in material design: chemically programmed synthesis of zeolitic imidazole framework-8†

Norbert Német,[a] Gábor Holló,[b] Gábor Schuszter, [iD][c] Dezső Horváth, [iD][d] Ágota Tóth, [iD][c] Federico Rossi [iD][e] and István Lagzi [iD] *[ab]

Here we show a time-programmed and autonomous synthesis of zeolitic imidazole framework-8 (ZIF-8) using a methylene glycol–sulfite clock reaction. The induction period of the driving clock reaction, thus, the appearance of the ZIF-8 can be adjusted by the initial concentration of one reagent of the chemical clock. The autonomously synthesized ZIF-8 showed excellent morphology and crystallinity.

Metal–organic frameworks (MOFs) are unique 2D or 3D hierarchical porous materials self-assembled from metal cations and organic linkers.[1,2] MOFs have been used in gas storage,[3–5] gas separation,[5,6] chromatography,[7,8] heterogeneous catalysis,[9,10] and targeted drug delivery.[11,12] The recent trend is that various MOFs have been applied in electronic applications since they have special and unique charge transport properties.[13,14] There are several synthetic routes that have been exploited to generate MOF structures. The most robust and firstly developed technique is the solvothermal method, in which metal salts and organic linkers are dissolved in a solvent and mixed in a reactor. The common solvents used include *N,N*-dimethylformamide (DMF), *N,N*-diethylformamide (DEF), methanol, and acetonitrile.[15–17] The temperature of the synthesis is generally greater than the room temperature. Later, other powerful techniques have been developed such as electrochemical,

hydrothermal, mechanochemical, microwave-assisted, and flow-driven routes.[18–22]

In the framework of environmental sustainability, there is an increasing demand to develop green synthesis methods to generate high stability and high porosity MOF crystals using water as a solvent. Moreover, an aqueous environment allows to take advantage of the aqueous acid–base chemistry to gain better control over the environmental conditions and would permit to implement smart synthetic routes by employing known autonomous chemical systems.

Using these systems (such as clock reactions, enzymatic reactions) to drive the self-assembly of various components and supramolecular gelation has recently gained much interest due to its versatile applicability.[23–30] The main idea in these applications is that the building blocks of the system (such as nanoparticles, polymers, macromolecules) are sensitive to the response generated by the autonomous driving system (pH, redox potential, concentration of the product).[31–34] It should be noted that usually, these driving systems contain harsh (*e.g.*, oxidative) initial reagents and intermediate products that may interfere with the building blocks limiting the applicability of these autonomous systems.[35] Therefore, the application of autonomous chemical reactions in materials synthesis and design remains challenging. However, the application of these reactions may provide two very important benefits for the synthesis. First, the process is autonomous and starts after a given time (induction period) that can be efficiently programmed by adjusting the experimental conditions (concentration of the initial reagents, temperature). This differs from the regular synthesis methods, in which the synthesis starts immediately after mixing the reagents. Secondly, in classical approaches, the experimental factors such as temperature, pH, and solvent composition remain fixed in the course of the synthesis. In chemical clock-type reactions (including autocatalytic and enzymatic reactions) the concentration of the products (for example, the concentration of the hydrogen ions, *i.e.*, pH) and the rate of its change, which drive the synthesis, change continuously in time. The rate of the concentration change in the

[a] *Department of Physics, Institute of Physics, Budapest University of Technology and Economics, H- 1111Műegyetem rkp 3., Budapest, Hungary*

[b] *MTA-BME Condensed Matter Research Group, Budapest University of Technology and Economics, H-1111Műegyetem rkp 3., Budapest, Hungary.*
E-mail: lagzi.istvan.laszlo@ttk.bme.hu; Fax: +361463-3567; Tel: +361463-1341

[c] *Department of Physical Chemistry and Materials Science, University of Szeged, H-6720 Rerrich Béla tér 1, Szeged, Hungary*

[d] *Department of Applied and Environmental Chemistry, University of Szeged, H-6720, Rerrich Béla tér 1, Szeged, Hungary*

[e] *Department of Earth, Environmental and Physical Science – DEEP Sciences, University of Siena, Pian dei Mantellini 44, 53100 Siena, Italy*

† Electronic supplementary information (ESI) available: experimental details, formation of ZIF-8 in the aqueous phase, and supplementary figures, tables and references. See DOI: https://doi.org/10.1039/d2cc01139e

course of the clock reaction can be precisely controlled by the initial concentration of the reagents and experimental conditions. We can hypothesize that both continuous concentration change and the rate of the concentration change might favorably affect the regimes of the synthesis (*e.g.*, nucleation and growth).

In this work, we present an autonomous chemical system that can be used to drive the synthesis of new materials or to reinterpret and improve established synthesis methods. To prove our design concept, we show a chemically coded and time-programmed synthesis of zeolitic imidazole framework-8 (ZIF-8) using the methylene glycol–sulfite clock reaction[36–39] as a driver of the process in the aqueous phase. We chose ZIF-8 because it is one of the most known representative molecules within MOFs, and it has been extensively studied in the past.[40] Therefore, it serves as a model system for the generation of other MOFs.

All experiments were carried out in a batch setup (round glass cuvette, V = 24 mL) by mixing four solutions to produce the given concentrations of the chemical species in the reactor: (i) sodium sulfite/sodium bisulfite buffer ($[SO_3^{2-}]_0$ = 5 – 60 mM, $[HSO_3^-]_0$ = 1200 mM); (ii) 2-Methylimidazole (2-Met) solution ($[2\text{-Met}]_0$ = 100 mM); (iii) zinc sulfate solution ($[Zn^{2+}]_0$ = 2 mM) and (iv) formaldehyde solution (1200 mM) (which contained in one case glucono-δ-lactone (100 mM)). The contents of the reactor were continuously stirred by using a magnetic stirrer at 350 rpm. The pH and the turbidity change in the cuvette were monitored by a pH electrode (Mettler Toledo) and UV-Vis spectrophotometer (VWR UV-1600 PC) at room temperature (22 ± 0.5 °C), respectively (for details see the ESI†). At the beginning of the methylene glycol–sulfite reaction (induction period, first stage), the pH changed slowly due to the buffer capacity of the sulfite/bisulfite system. When all the buffer is consumed, the pH suddenly increases by jumping roughly 4 pH units due to the reaction of sulfite with methylene glycol (second stage). A high excess of 2-Met was used in the experiments because this ensured the formation of ZIF-8 in the aqueous environment.[41]

The autocatalytic reaction started at pH $\sim$ 5.5, at this acidic range the formation of ZIF-8 did not occur. However, once the pH reached ~ 8.5, the generation of ZIF-8 particles started as manifested by the turbidity increase of the samples (Fig. 1). Further pH increase involved further turbidity change. However, once the pH reached a plateau, the turbidity stopped increasing after some time depending on the concentration of the sulfite, showing that the formation of ZIF-8 was driven by the methylene glycol–sulfite autocatalytic reaction. We carried out a control experiment to investigate whether the chemical clock reaction is the driving phenomenon in the time-programmed synthesis. The solutions of zinc and 2-Met were mixed and stirred continuously. The turbidity change started only at $\sim$ 90 min even though the initial pH was 9.3 and it dropped by 0.3 units (Fig. S1, ESI†). The explanation of this observation can be that at higher (alkaline) pH the concentration of the zinc-protonated 2-Met complex (which is a precursor of ZIF-8) is higher than at the slightly acidic range (where the double protonated form of 2-Met is dominant).[41] This high concentration causes high supersaturation which resulted in small ZIF-8 nuclei (having no Mie-scattering) which grow further slowly in time providing a shift in the turbidity. However, when the pH gradually increases by the clock reaction from the acidic region, at pH when sufficient protonated 2-Met are present, the concentration of the complex is lower, thus lower supersaturation results in bigger particles which is manifested in the faster appearance of turbidity.

High initial concentrations of bisulfite and formaldehyde were used compared to the system with the absence of 2-Met[37] because of the base hydrolysis of 2-Met. Fig. S2 (ESI†) presents the effect of the initial concentration of the formaldehyde on the induction period and pH change generated by the clock reaction.

There are two important features that should be discussed. First, it can be seen that the induction time (defined as the time to reach the highest reaction rate, measured from the beginning of the experiment) varied with a trend in the experiments. In our setup, it ranged between 7 and 22 s depending on the
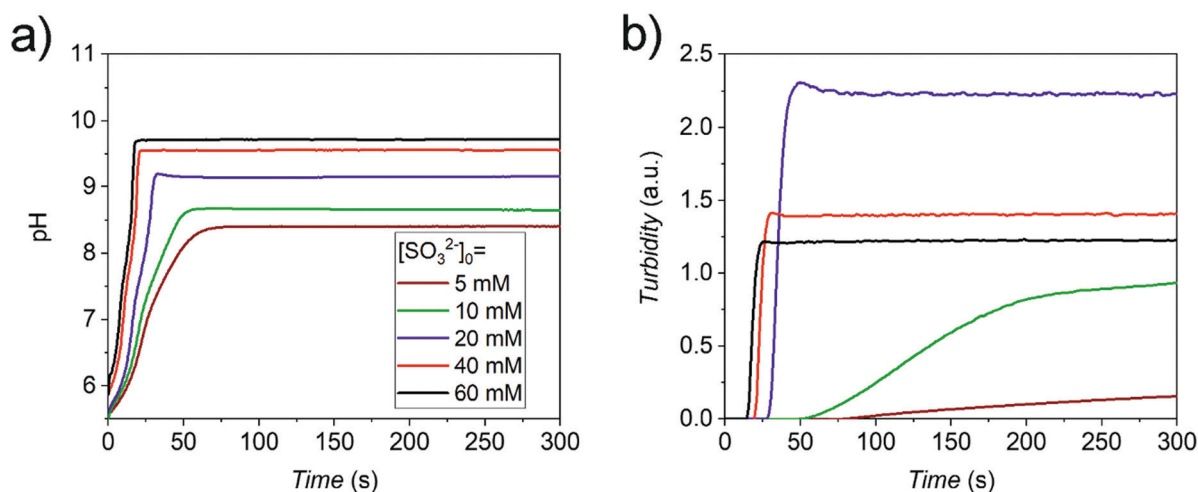

Fig. 1 Time-resolved pH (a) and turbidity (b) (defined as absorbance at λ = 600 nm) curves of the methylene glycol–sulfite reactions in the presence of zinc ions ($[Zn^{2+}]_0$ = 2 mM) and 2-methylimidazole ($[2\text{-Met}]_0$ = 100 mM) using various initial sulfite concentrations (5, 10, 20 40, and 60 mM) in experiments.

initial concentration of the reagents; here, we changed the concentration of the sulfite. Higher sulfite concentration resulted in a shorter induction period and faster appearance of the ZIF-8 particles (Fig. S3, ESI†). In this manner, since the ZIF-8 synthesis is pH-dependent, the start of the generation of ZIF-8 particles can be feasibly manipulated autonomously. It should be noted that at lower concentrations of the sulfite, the maximum rates of both pH and turbidity changes were low. The maximum rate of the pH change increased with the sulfite concentration. However, the maximum rate of the turbidity change at higher sulfite concentrations ($[SO_3^{2-}]_0 > 20$ mM) remained constant (Fig. S4, ESI†). Secondly, one can observe a counterintuitive trend. A continuous increase of the sulfite concentration generated higher pH and higher turbidity of the samples. However, when the concentration reached $[SO_3^{2-}]_0 = 20$ mM, we obtained the highest turbidity (Fig. 1b), its further increase generated higher pH, but lower turbidity. This can be explained by a concurrent process, namely the formation of zinc hydroxide and its complexes. At this range, higher pH generates more zinc hydroxide and zinc hydroxo-complexes (Fig. S5, ESI†).

To characterize the morphology and crystalline structure of the synthesized ZIF-8 crystals, we performed scanning electron microscopy (SEM) and powder X-ray diffraction (PXRD) measurements (Fig. 2 and Fig. S6, ESI†). To use this chemically driven approach to synthesize other materials, it is inevitably important to examine and study the side effects that originated from the driving system. The SEM analysis of the samples revealed that the optimal conditions for the formation of ZIF-8 crystals are at moderate sulfite concentration ($[SO_3^{2-}]_0 = 20$ mM), (Fig. S6, ESI†). In this case, the PXRD pattern revealed an excellent crystallinity of the formed crystals (Fig. 2b). At low sulfite concentrations ($[SO_3^{2-}]_0 < 20$ mM), the generated lower pH did not create an optimal condition for the formation of dodecahedral ZIF-8 crystals (Fig. S6a and b, ESI†). At high sulfite concentrations ($[SO_3^{2-}]_0 > 20$ mM), the morphology of the crystals differs from the dodecahedral shape (round shape crystals) compared to the morphology of the crystals obtained at $[SO_3^{2-}]_0 = 20$ mM (Fig. S6d and e, ESI†). We carried out control synthesis experiments in the absence of the clock reaction and observed the formation of plate-like crystals, which may correspond to the formation of the diamondoid topology (Fig. S7, ESI†).[42] Based on this result and the time domain of the clock reaction, we can conclude that the clock reaction can control the nucleation event rather than the crystal growth.

To illustrate our design concept, we developed a kinetic model that successfully reproduced the experimentally observed trend (Fig. S8, ESI†). The model contains the methylene glycol–sulfite autocatalytic reaction mechanism coupled to the formation of ZIF-8 and zinc hydroxide, and its complex formation in the excess of base (see ESI† for details). The generation of ZIF-8 in the aqueous phase significantly differs from the reaction steps in polar protic and aprotic solvents due to the different deprotonation mechanisms of 2-Met (MIMH).[43,44] These solvents themselves act as deprotonating
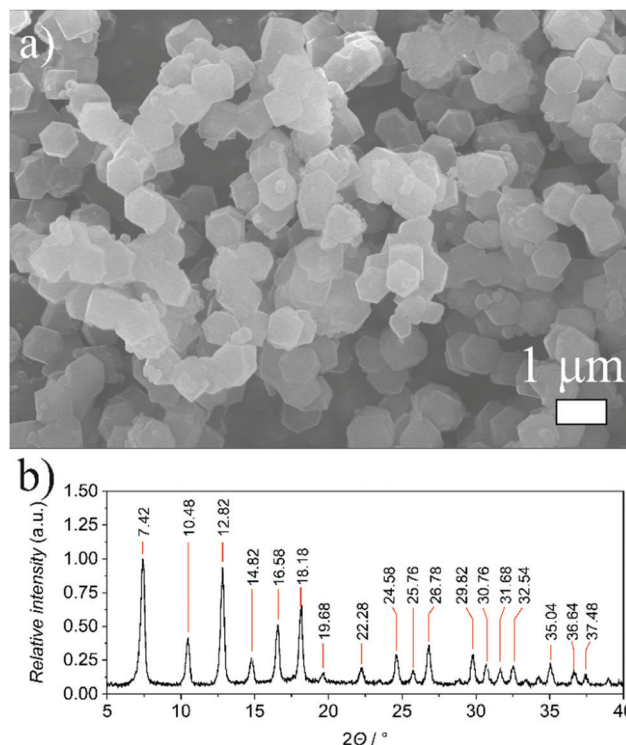

Fig. 2 SEM micrographs (a) and PXRD pattern (b) of the synthesized ZIF-8 crystals using the methylene glycol–sulfite clock reaction using $[SO_3^{2-}]_0 = 20$ mM ($[HCOH]_0 = 1300$ mM, $[HSO_3^-]_0 = 1200$ mM, $[Zn^{2+}]_0 = 2$ mM, and $[2\text{-}Met]_0 = 100$ mM).

agents. However, in the aqueous phase, the mechanism is more complicated since the deprotonation of 2-Met (MIMH) does not occur even at a higher alkaline range because of its high pK_a value (pK_a was reported between 14 and 15).[41,43] The discussion of the formation of ZIF-8 in the aqueous phase can be found in the ESI.†

Our kinetic model could reproduce qualitatively two key features observed in experiments, namely the delayed formation of ZIF-8 and the maximum yield of ZIF-8 at moderate sulfite concentration (Fig. S8, ESI†). The kinetic model explains the latter phenomenon. At lower pH regions generated by the clock reaction (using low initial sulfite concentrations), the concentration of the zinc hydroxide and its complexes are relatively lower (i.e., more ZIF-8 can be generated). However, after a certain pH, any further pH increase generates a greater amount of zinc hydroxo-complexes in the system thus the concentration of the ZIF-8 (turbidity in the experiments) decreases even though the pH was increased (Fig. S8, ESI†).

The methylene glycol–sulfite autocatalytic reaction coupled with the hydrolysis of a lactone (e.g., glucono-δ-lactone) can generate a subsequent pH decrease in the system.[31,38,39] Since the formation of ZIF-8 is reversible and pH-dependent, using this system, we could present a delayed formation and dissolution of the formed ZIF-8 (Fig. S9a, ESI†). ZIF-8 disintegrated at pH ~ 8.5 which was perfectly captured by the extended kinetic model (Fig. S9b, ESI†). The time-domain of the existence of ZIF-8 in this system is short (~ 20 s), however, it can be expanded by

using lactones having a slower hydrolysis rate (*e.g.*, δ-valerolactone).[31] This result might help to design MOF oscillators in which the autonomous pH oscillators could drive the reversible formation of MOF structures.

In conclusion, we have shown that a time-programmed and autonomous synthesis of ZIF-8 can be realized by using the methylene glycol–sulfite chemical clock. In the induction period, the pH is not high enough to initiate and drive the synthesis of ZIF-8, *i.e.*, the system is in a dormant state. The synthesis starts once the pH reaches a threshold value. The induction period and, therefore, the start of the formation of ZIF-8 crystals can be controlled by the concentration of one reagent (sulfite). We have found that in an optimal case, the formed crystals have excellent crystallinity, and the driving chemical system controlled the formation of ZIF-8. Our results can open up new routes in the application of non-linear chemical reaction networks in material synthesis.

Conflicts of interest

There are no conflicts to declare.

Notes and references

1 H.-C. Zhou, J. R. Long and O. M. Yaghi, *Chem. Rev.*, 2012, **112**, 673–674.
2 H. Li, M. Eddaoudi, M. O'Keeffe and O. M. Yaghi, *Nature*, 1999, **402**, 276–279.
3 L. J. Murray, M. Dincǎ and J. R. Long, *Chem. Soc. Rev.*, 2009, **38**, 1294–1314.
4 D. Alezi, Y. Belmabkhout, M. Suyetin, P. M. Bhatt, J. Weseliński, V. Solovyeva, K. Adil, I. Spanopoulas, P. N. Trikalitis, A.-H. Emwas and M. Eddaoudi, *J. Am. Chem. Soc.*, 2015, **137**, 13308–13318.
5 H. Li, L. Li, R.-B. Lin, W. Zhou, Z. Zhang, S. Xiang and B. Chen, *EnergyChem*, 2019, **1**, 100006.
6 J.-R. Li, R. J. Kuppler and H.-C. Zhou, *Chem. Soc. Rev.*, 2009, **38**, 1248–1256.
7 S. Han, Y. Wei, C. Valente, I. Lagzi, J. J. Gassensmith, A. Coskun, J. F. Stoddart and B. A. Grzybowski, *J. Am. Chem. Soc.*, 2010, **132**, 16358–16361.
8 Y. Yu, Y. Ren, W. Shen, H. Deng and Z. Gao, *TrAC, Trends Anal. Chem.*, 2013, **50**, 33–41.
9 J. Y. Lee, O. K. Farha, K. A. Scheidt, S. B. T. Nguyen and J. T. Hupp, *Chem. Soc. Rev.*, 2009, **38**, 1450–1459.
10 L. Ma, C. Abney and W. Lin, *Chem. Soc. Rev.*, 2009, **38**, 1248–1256.
11 M.-X. Wu and Y.-W. Yang, *Adv. Matter*, 2017, 1606134.
12 P. Horcajada, T. Chalati, C. Serre, B. Gillet, C. Sebrie, T. Baati, J. F. Eubank, D. Heurtaux, P. Clayette, C. Kreuz, J.-S. Chang, Y. K. Hwang, V. Marsaud, P.-N. Bories, L. Cynober, S. Gil, G. Férey, P. Couvreur and R. Gref, *Nat. Mater.*, 2010, **9**, 172–178.
13 J. J. Calvo, S. M. Angel and M. C. So, *APL Mater.*, 2020, **8**, 050901.
14 M. Shen, Y. Zhang, H. Xu and H. Ma, *iScience*, 2021, **24**, 103069.
15 R. Seetharaj, P. V. Vandana, P. Arya and S. Mathew, *Arabian J. Chem.*, 2019, **12**, 295–315.
16 J. G. Flores, M. Díaz-García, I. A. Ibarra, J. Aguilar-Pliego and M. Sánchez-Sánchez, *J. Solid State Chem.*, 2021, **298**, 122151.
17 S. Leubner, R. Stäglich, J. Franke, J. Jacobsen, J. Gosch, R. Siegel, H. Reinsch, G. Maurin, J. Senker, P. G. Yot and N. Stock, *Chem. – Eur. J.*, 2020, **26**, 3877–3883.
18 R. S. Kumar, S. S. Kumar and M. A. Kulandainathan, *Microporous Mesoporous Mater.*, 2013, **168**, 57–64.
19 W. Chen, L. Du and C. Wu, in *Metal-Organic Frameworks for Biomedical Applications*, Elsevier, 2020, 141–157.
20 D. Chen, J. Zhao, P. Zhang and S. Dai, *Polyhedron*, 2019, **162**, 59–64.
21 J. Klinowski, F. A. A. Paz, P. Silva and J. Rocha, *Dalton Trans.*, 2011, **40**, 321–330.
22 Z. Liu, J. Zhu, C. Peng, T. Wakihara and T. Okubo, *React. Chem. Eng.*, 2019, **4**, 1699–1720.
23 L. Heinen and A. Walther, *Soft Matter*, 2015, **11**, 7857–7866.
24 T. Heuser, A.-K. Steppert, C. Molano Lopez, B. Zhu and A. Walther, *Nano Lett.*, 2015, **15**, 2213–2219.
25 T. Heuser, E. Weyandt and A. Walther, *Angew. Chem., Int. Ed.*, 2015, **54**, 13258–13262.
26 E. Jee, T. Bánsági, A. F. Taylor and J. A. Pojman, *Angew. Chem., Int. Ed.*, 2016, **55**, 2127–2131.
27 G. Panzarasa, T. Sai, A. L. Torzynski, K. Smith-Mannschott and E. R. Dufresne, *Mol. Syst. Des. Eng.*, 2020, **5**, 445–448.
28 G. Panzarasa, A. L. Torzynski, T. Sai, K. Smith-Mannschott and E. R. Dufresne, *Soft Matter*, 2020, **16**, 591–594.
29 S. Riedel, T. Schweizer, K. Smith-Mannschott, E. R. Dufresne and G. Panzarasa, *Soft Matter*, 2021, **17**, 1189–1193.
30 C. C. M. Sproncken, B. Gumí-Audenis, G. Panzarasa and I. K. Voets, *ChemSystemsChem*, 2020, **2**, 2000005.
31 E. Tóth-Szeles, J. Horváth, G. Holló, R. Szűcs, H. Nakanishi and I. Lagzi, *Mol. Syst. Des. Eng.*, 2017, **2**, 274–282.
32 I. Lagzi, B. Kowalczyk, D. Wang and B. A. Grzybowski, *Angew. Chem., Int. Ed.*, 2010, **49**, 8616–8619.
33 T. Liedl and F. C. Simmel, *Nano Lett.*, 2005, **5**, 1894–1898.
34 H. Nabika, T. Oikawa, K. Iwasaki, K. Murakoshi and K. Unoura, *J. Phys. Chem. C*, 2012, **116**, 6153–6158.
35 N. Német, Y. Miele, G. Shuszter, E. L. Tóth, J. E. Maróti, P. J. Szabó, F. Rossi and I. Lagzi, *React. Kinet., Mech. Catal.*, 2022, **135**, 15–28.
36 P. Warneck, *J. Chem. Educ.*, 1989, **66**, 334–335.
37 K. Kovacs, R. McIlwaine, K. Gannon, A. F. Taylor and S. K. Scott, *J. Phys. Chem. A*, 2005, **109**, 283–288.
38 K. Kovacs, R. E. McIlwaine, S. K. Scott and A. F. Taylor, *J. Phys. Chem. A*, 2007, **111**, 549–551.
39 K. Kovacs, R. E. McIlwaine, S. K. Scott and A. F. Taylor, *Phys. Chem. Chem. Phys.*, 2007, **9**, 3711–3716.
40 T. D. Bennett, S. Cao, J. C. Tan, D. A. Keen, E. G. Bithell, P. J. Beldon, T. Friscic and A. K. Cheetham, *J. Am. Chem. Soc.*, 2011, **133**, 14546–14549.
41 K. Kida, M. Okita, K. Fujita, S. Tanaka and Y. Miyake, *CrystEngComm*, 2013, **15**, 1794.
42 Z. Akimbekov, A. D. Katsenis, G. P. Nagabhushana, G. Ayoub, M. Arhangelskis, A. J. Morris, T. Friščić and A. Navrotsky, *J. Am. Chem. Soc.*, 2017, **139**, 7952–7957.
43 Z. Shi, Y. Yu, C. Fu, L. Wang and X. Li, *RSC Adv.*, 2017, **7**, 29227–29232.
44 M. Jian, B. Liu, R. Liu, J. Qu, H. Wang and X. Zhang, *RSC Adv.*, 2015, **5**, 48433–48441.